Heliyon 7 (2021) e07796

Contents lists available at ScienceDirect

Heliyon

journal homepage: www.cell.com/heliyon

Research article

Electronic structure transition of cubic $CsSnCl_3$ under pressure: effect of rPBE and PBEsol functionals and GW method

Md. Majibul Haque Babu [a,b], Tusar Saha [a], Jiban Podder [a], Protima Roy [a], Abdul Barik [a], Enamul Haque [c,*]

[a] Department of Physics, Bangladesh University of Engineering and Technology, Dhaka, 100, Bangladesh
[b] Basic Science Division, World University of Bangladesh, Dhaka, 1205, Bangladesh
[c] EH Solid State Physics Laboratory, Longaer, Gaffargaon, 2233, Mymensingh, Bangladesh

ARTICLE INFO

Keywords:
First-principles calculations
Pressure effect
Bandgap tuning
Semiconductor-metallic transition
Absorption
Mechanical properties

ABSTRACT

The antiperovskites based on metal halides have emerged as potential materials for advanced photovoltaic and electronic device applications. But the wide bandgap of non-toxic $CsSnCl_3$ reduces its photovoltaic efficiency. Here, we report the change of electronic structure of $CsSnCl_3$ at different pressure by using GGA-rPBE and GGA-PBEsol functionals and the GW method. We have shown that the prediction of electronic structure transition (semiconducting to metallic state) strongly depends on the exchange-correlation and the GW method gives the most reasonable values of the bandgap under pressure. The pressure increases the electronic density of states close to the Fermi level by pushing the valence electrons upward and thus, reduces the bandgap linearly. Afterward, we have also investigated the influence of pressure on absorption coefficient, and mechanical properties meticulously. Although the pressure shifts the absorption peak to lower photon energies, the absorption coefficient is slightly improved.

1. Introduction

In the cutting-edge world, the synthesis of air and moisture-stable compounds are playing a significant role in the fabrication of high-performance devices. Importantly, a diversity of compounds and alloys is accessible, but the stability and physical properties impose restrictions on their use in technological devices. To resolve the problem, however, researchers are searching for air and moisture stable materials with useful properties in the required surrounding conditions. Some perovskites are air and moisture stable with useful physical properties for solar cell applications [1, 2]. Besides, these compounds show insulator, conductor, semiconductor, and superconductor properties as well [1, 2]. They have noteworthy physical properties including optical, charge ordering, magnetic, useful spin-dependent electronic transport, good thermoelectric performance, high magnetoresistance, and ferroelectric properties [3, 4, 5, 6, 7]. Recently, the physical properties of metal halide perovskite (AMX_3, where A, M, and X represent a cation, metal (ion), and halogen (anion) respectively) materials have been investigated extensively as it has possessed several salient optoelectronic properties such as tunable optical bandgap, absorption spectrum in a wide range, narrow emission width, large numbers of mobile carriers with light effective mass, and high absorption and charge diffusion [8, 9]. Most importantly, it is abundant with low-cost precursor solutions on everywhere place in the world. To date, ABX_3 has been applied to different electronic devices including light-emitting diodes (LEDs), photovoltaics (PVs), and fuel cells [8].

The application of hydrostatic pressure or strain engineering has arisen as an effective means of tuning the physical properties of ABX_3 materials such as structural phases and electronic band structure, which provides a better understanding of the change in the rigid bonding [10, 11, 12]. In the conduction band maximum (CBM) of ABX_3 perovskites, the 'X-*p* and 'B-*p* orbitals have dominant contributions, while valence band maximum (VBM) contributions come from 'X'-*p*, 'B'-*s* and 'B'-*p* orbitals [13]. On the other hand, the cation 'A' does not have a significant effect on the bandgap, but it mediates the metal halide interactions [14]. Besides, the bandgap is associated with the lattice parameters of the ABX_3 perovskite structure which signifies the significance of octahedral tilting upon the optical properties of ABX_3 perovskites [15]. As a result, the optimized band gaps of ABX_3 perovskites are obtained, rises charge carrier life-times, diminishes trap state densities, and tunes carrier

* Corresponding author.
E-mail address: enamul.phy15@yahoo.com (E. Haque).

https://doi.org/10.1016/j.heliyon.2021.e07796
Received 15 May 2021; Received in revised form 1 July 2021; Accepted 12 August 2021

conductivities. So, it is increasingly being used in p-n junctions, photovoltaic, and electronic devices [16].

Recently, the effects of hydrostatic pressure on the physical properties of metal halide ABX_3 perovskites were studied meticulously, for example, $CsGeBr_3$ and $CsGeI_3$ [17, 18, 19]. $CsGeCl_3$ has been also examined but not precisely. Internal and external pressure in cubic ABX_3 perovskite have been examined using HSE + SOC function by Metin et al. and reported that there is no phase transition, and the bandgap shrinkage with increasing internal pressure while bandgap increases by external pressure [13]. Conversely, Jakiul et al. reported that they have found semiconductor to metallic transition at 20 GPa using GGA + PBE function, and an identical scissor value (1.857 eV) is taken from the experimental value for each pressure, which is completely wrong [19]. Besides, Ying et al. reported that the optical band gap reveals red-shifts and blue shifts with 3D topological non-trivial phase and band inversion by tuning the hydrostatic pressure [20]. But they did not much explain the bond length. Thus, there is still needed a convincible investigation of $CsSnCl_3$ materials under pressure and to find out the correlation between bond length and phase transition.

Therefore, the aim of our present study further investigates the physical properties of $CsSnCl_3$ materials accurately and detects association with the bond length and phase transition through GGA + PBEsol, GGA + rPBE functionals, and GW method. For the first time, we have calculated the electronic structure, absorption coefficient of $CsSnCl_3$ under different pressures by using the GW method.

2. Computational methods

The structural relaxations were performed by using density functional theory (DFT) within the plane-wave pseudopotential technique implemented in CASTEP (Cambridge Serial Total Energy Package) code [21, 22] by minimizing energy and interatomic forces simultaneously. For this, we initially used the experimental lattice parameters and atomic coordinates. We set strict convergence criteria, energy 10^{-6} eV and force 10^{-3} eV/Au. We treated the exchange-correlation energy term by using the generalized gradient approximation (GGA) with Perdew-Berke-Ernzerhof for solids (PBEsol) and revised Perdew-Berke-Ernzerhof (rPBE) settings. We used Vanderbilt ultrasoft pseudopotentials [23] and the BFGS (Broyden–Fletcher–Goldfarb–-Shanno) technique [24] with the cutoff energy 550 eV with $12 \times 12 \times 12$ Monkhorst–Pack [25] after extensive trials. The calculations of elastic constants were accomplished by using finite-strain theory [26] as implemented in CASTEP. For GW calculations, we used the plane-wave pseudopotential (PW) method, like that of CASTEP, in Quantum Espresso (QE) code [27]. We set the same convergence criteria as mentioned above and used Optimized norm-conserving Vanderbilt pseudopotentials [28, 29] and $2 \times 2 \times 2$ k-point, as the calculations are very expensive. For the self-consistent calculations, we used PBEsol functional by using the above settings and calculated self-consistent potentials. By using this potential, we calculated Quasi-Particle energy implemented in BerkeleyGW code [30]. Then, the G_0W_0 electronic structure calculations were performed by using the above outputs. In all calculations, we did not consider spin-orbit interactions, as these calculations with spin-orbit interactions are much expensive.

3. Results and discussion

The ground state cubic structure of $CsSnCl_3$ is depicted in Figure 1. The Cesium tin chlorides ($CsSnCl_3$) have an ideal cubic structure having space group $Pm\bar{3}m$ (no. 221) [31]. Where, Cs atoms lie at the corner of the unit cell with 1a (0, 0, 0) Wyckoff position, Sn atom occupies the body-centered 1b $\left(\frac{1}{2}, \frac{1}{2}, \frac{1}{2}\right)$, Wyckoff position, and Cl atom at the face-centered $\left(0, \frac{1}{2}, \frac{1}{2}\right)$ Wyckoff positions [31].

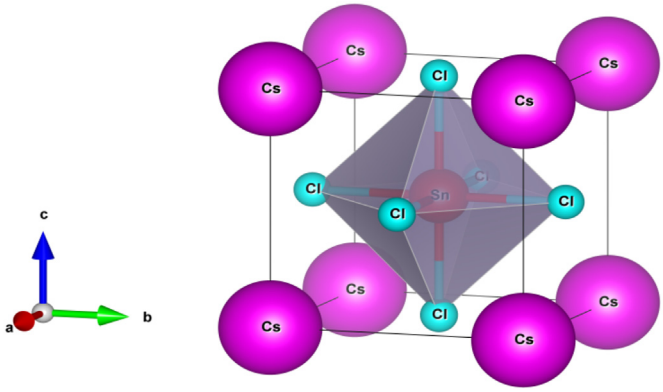

Figure 1. A ground-state crystal structure of $CsSnCl_3$ compound.

The different functionals treat the exchange-correlation term differently and the calculated lattice parameters vary slightly depending on the type of function. That's why the geometric optimization of the $CsSnCl_3$ structure has been performed by using different functionals, namely i.e PBEsol and rPBE. The PBEsol and rPBE functionals give the lattice parameters, of $CsSnCl_3$, 5.51, and 5.75 Å, respectively, while the experimental value is 5.56[31]. Like PBE functional, rPBE also overestimates the experimental value, while as usual, the PBEsol underestimates the experimental lattice parameters slightly.

It, however, can be seen (also Figure 2) that the effects of hydrostatic pressures have great influences on the lattice parameters, volumes, and bond lengths (Cs–Cl, and Cl–Sn) in both PBEsol and rPBE method as demonstrated in Figure 2, which did not manifest by Zakiul et al [19]. The hydrostatic pressure gradually declines the lattice parameters by reducing the interatomic distance. Interestingly, both functionals calculate a longer bond length of Cs–Cl than Cl–Sn. These three types of bond lengths are deteriorated moderately by employing hydrostatic pressure due to the production of compressive strain within the $CsSnCl_3$ lattice network. This suggests that the change in bond lengths would profoundly inspiration the electronic structures of the $CsSnCl_3$ compound. The detailed changes of these bond lengths are shown in Figure 2 (c, d).

3.1. Electronic properties

The accuracy of the calculation of electronic bandgap strongly depends on the type of functionals. Generally, GGA with different settings underestimates the experimental bandgap. To demonstrate this, we have calculated the electronic structure of $CsSnCl_3$ by using PBEsol and rPBE functionals. The computed band structures, by using PBEsol and rPBE, of $CsSnCl_3$ at ambient conditions and different pressures are shown in Figures 3 and 4, respectively.

The gross features of the electronic dispersions of $CsSnCl_3$ are almost the same for both functionals. The PBEsol functional is less effective to compensate for self-interaction energy. Thus, shifted the minima of the conduction band downward and underestimates the bandgap severely. On the other hand, the rPBE functional improves the bandgap but it still underestimates the experimental bandgap largely. At ambient conditions, the computed bandgap of $CsSnCl_3$ is 0.55 and 1.4 eV by using PBEsol and rPBE functional, while the experimentally measured bandgap is 2.9 eV [32].

The pressure excites the valence electrons upward. It pushes the conduction band minima downward and Fermi levels upward. Thus, the bandgap is reduced with the pressure linearly. The gap is disappeared above 4 GPa and 8 GPa for PBEsol and rPBE functional, respectively. However, the bandgap can be correlated with the change of bond length while applying various hydrostatic pressures (see Figure 2 c, d). The $CsSnCl_3$ shows a metallic band structure when the bond length reaches a certain limit. In PBEsol functional, the $CsSnCl_3$ shows a metallic band structure when the bond lengths of Cs–Cl and Cl–Sn are at or below 3. 74

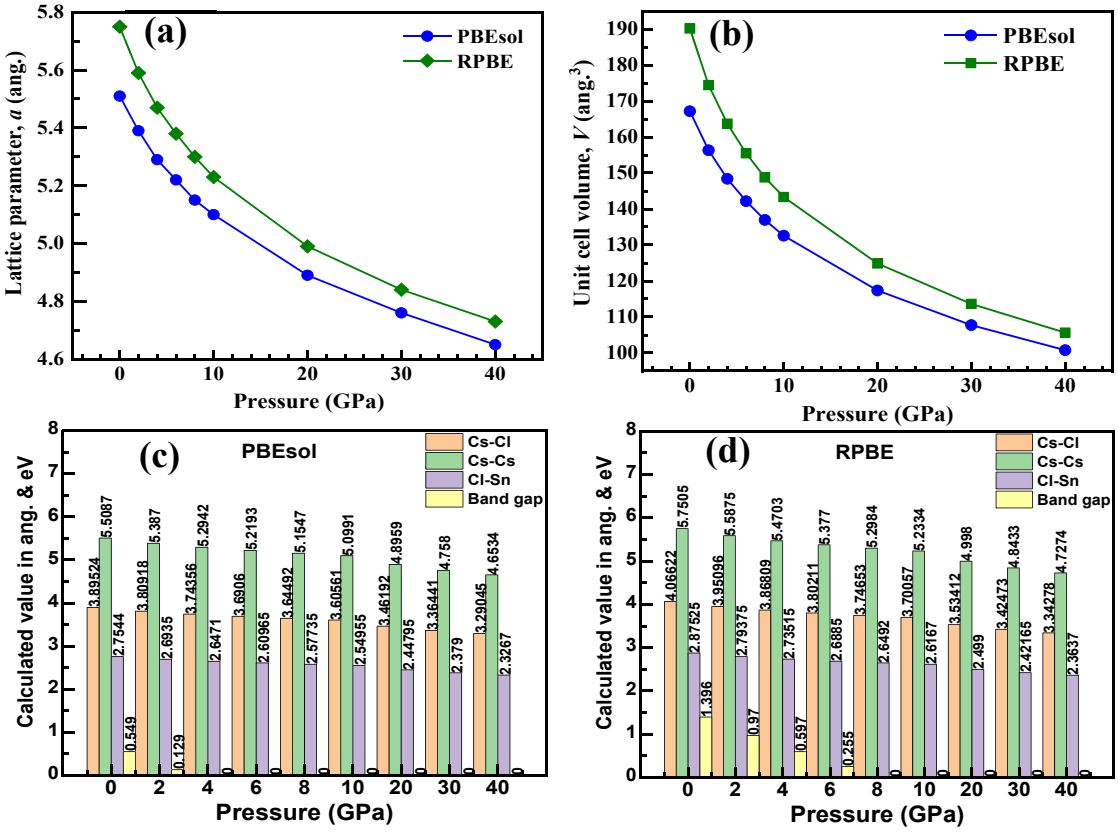

Figure 2. Pressure-induced structural distortions in cubic $CsSnCl_3$ perovskite: (a) lattice constants (*a*), (b) unit cell volume (V), and (c, d) comparison study of several bond lengths, respectively.

and 2.64 Å, respectively. Likewise, in rPBE functional, $CsSnCl_3$ also develops a metallic band structure when Cs–Cl and Cl–Sn bond lengths reach the same limit (see Figure 2 d). This information may be useful for experimentalists to perform the Rietveld refinement analysis. The fact demonstrates how these functionals treat self-interaction energy and PBEsol is less effective than rPBE to compensate for self-interaction energy.

The electronic phase transition nature of the $CsSnCl_3$ perovskite under pressure can be further understood from the total electronic density of states (DOS) as shown in Figure 5 (a, b).

The DOS at the Fermi level rises significantly above 4 GPa for PBEsol and above 8 GPa for rPBE functional, suggesting semiconducting to a metallic electronic phase transition, which is consistent with the computed electronic band structures. As both functionals underestimate the bandgap severely, the prediction of metallic state at such pressure contains large uncertainty. Therefore, it is worth calculating the accurate bandgap of $CsSnCl_3$ by using a more sophisticated method available today.

That's why we have calculated the electronic band structures by using the GW method at four pressures 0, 20, 30, 40 GPa, as these calculations are very expensive. Figure 6 demonstrates the electronic dispersion relations of $CsSnCl_3$ perovskite under these pressures. The gross features of the electronic dispersions change slightly compared to that of PBEsol and rPBE functionals. Like PBEsol and rPBE functionals, the maxima of the valence band (VBM) and minima of the conduction band (CBM) remain at the high symmetry point R, while the excitation energy pushes the conduction bands upward, leading to a direct bandgap 2.91 eV at 0 GPa, which is excellent agreement with the experimental value 2.9 eV [32]. Note that the authors of Ref. [19] compared their calculated values and determined the scissor parameter from the experimental bandgap of the monoclinic $CsSnCl_3$ (2.8 eV from Ref. [33], although Refs. [32, 34] reported from spectrometric measurements that it is 4. 5 eV), which not correct. Interestingly, there is a small bandgap at 20 GPa and the valence band crosses the Fermi level at 30 GPa. The VBM and CBM almost touch the Fermi level at 30 GPa, but there is a still tiny bandgap (see Figure 5 b, c). After that, a metallic behavior is confirmed by 40 GPa. Therefore, it may be said that the bandgap of $CsSnCl_3$ perovskite would be around 1.3 below 10 GPa, suggesting that the compound under this condition would exhibit its best photovoltaic efficiency based on the Shockley–Queisser theory [35]. Further experimental studies are encouraged to explore the potential photovoltaic performance of $CsSnCl_3$ under pressure.

3.2. Optical properties

Solar is one of the most important eco-friendly energy resources and solar cell can convert solar energy into useful electricity. The performance of a solar cell is determined mainly by the absorption coefficient. The absorption coefficient measures the amount of light energy absorbed by a material. Thus, for high-performance solar cell applications, a material must have a high absorption coefficient.

The study of absorption coefficient is extremely vital to achieving deep information concerning the compatibility of materials for better performance device applications. For this reason, we have calculated the absorption coefficient of $CsSnCl_3$ and presented it graphically in Figure 7 (a,b). The compound possesses an intrinsically high absorption coefficient and pressure can only improve it slightly but shifts the peak to lower photon energy. As both functionals underestimate the values of the experimental bandgap severely, the calculated absorption coefficient might contain large uncertainties. Therefore, we need to calculate the absorption coefficient by using the GW method. However, the experimentally measured values of the bandgap of CsSnCl3 under pressure are not available, to date. Thus, we have calculated the absorption coefficient by GW method at ambient condition only and presented it graphically in Figure 7 (b). When the GW bandgap correction is applied to the

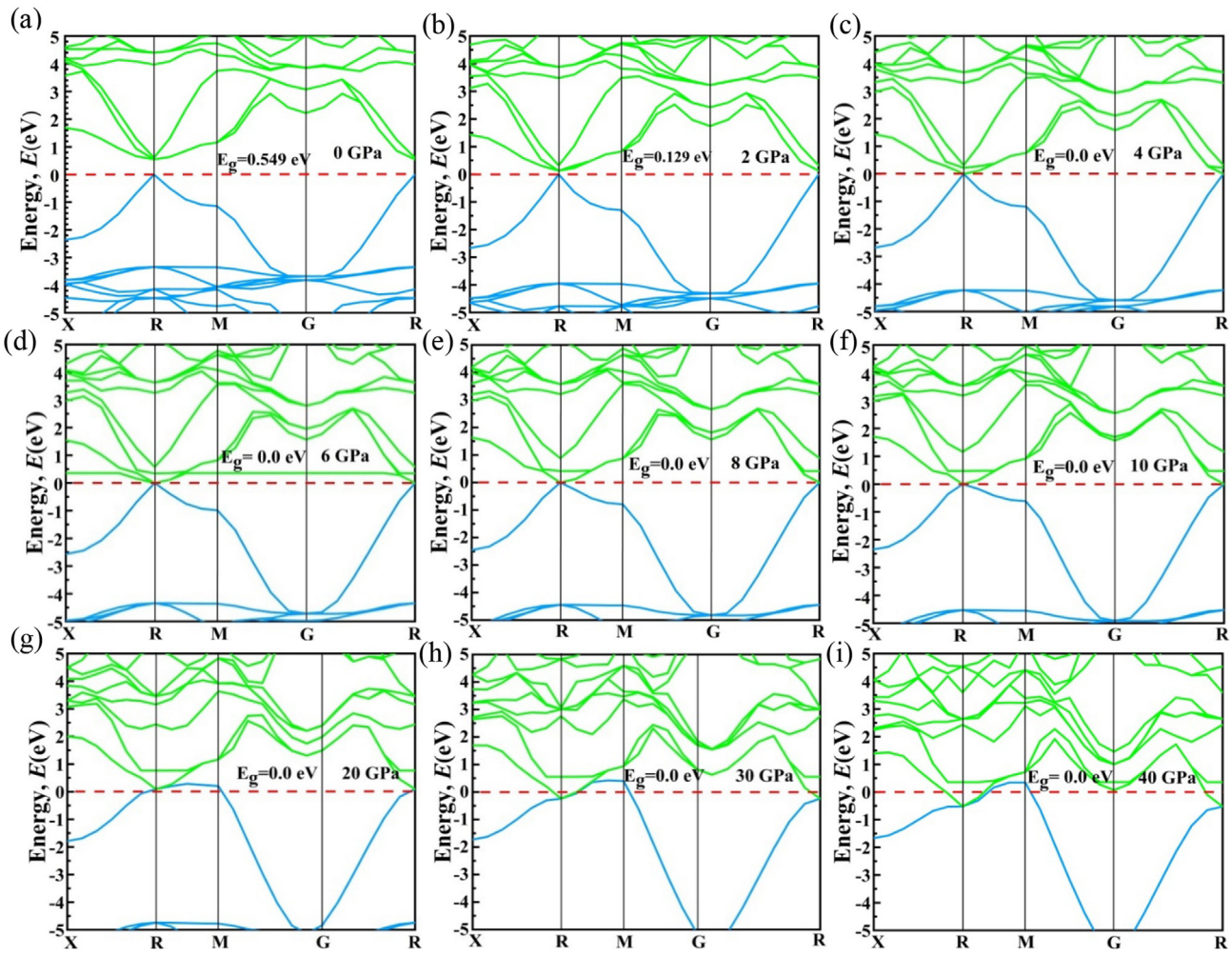

Figure 3. The computed band structure, by PBEsol functional, of $CsSnCl_3$ under different pressures: (a) 0 GPa, (b) 2 GPa, (c) 4 GPa, (d) 6 GPa, (e) 8 GPa, (f) 10 GPa, (g) 20 GPa, (h) 30 GPa, and (i) 40. The dashed line at the zero-energy represents the Fermi level.

absorption coefficient, the absorption changes significantly, and the peak shifts to the higher photon energy. The absorption of photons with energy ~6 eV is significant for the GW method. However, the value of the absorption coefficient does not rise significantly. This fact demonstrates the importance of accurate electronic structure calculations to describe the optical properties of material accurately.

3.3. Mechanical properties

Material suitability to external force is determined by elastic constant, enormously significant in potential implementation. So, we have explored the elastic stability of the perovskite compound $CsSnCl_3$ by pivotal parameter, elastic constants. Generalized Hook's law is used for determining the elastic constants of $CsSnCl_3$ [36]. According to Born–Huang's mechanical stability criterion, the strain energy should be positive. This stability criteria for the cubic system can be expressed as [37];

$$C_{11} > 0,\ C_{44} > 0,\ C_{11} + 2C_{12} > 0 \text{ and } C_{11}–C_{12} > \quad 0$$

Our calculated elastic constants by using PBEsol functional at different pressures are listed in Table 1. The computed values satisfy the stability criteria and hence, the compound is stable up to 30 GPa by using PBEsol functional within our computational accuracy. The mechanical instability appeared at 40 GPa with the PBEsol functional. The elastic constants C_{11}, C_{12}, and C_{44} are related to elasticity in length and shape, indicating how much it has deformed by applying various hydrostatic pressure. The C_{12} rises with pressure while C_{44} lowers with pressure. The Cauchy pressure also rises, suggesting that the ductility of the compound is improved by the applied pressure as listed in Table 1. The mechanical parameters such as a bulk modulus, B, shear modulus, G, Pugh's ratio, B/G ratio, and Poisson, v, are assessed based on prominent expressions as indicated in literature [38, 39] and listed in Tables 1, 2.

As the interatomic distance is reduced with pressure, the value bulk and shear moduli are increased with it. This indicates that the mechanical resistance of the $CsSnCl_3$ is substantially is improved under high pressure. In our exploration, the soft to hard transition occurred when the $CsSnCl_3$ material was subjected to different hydrostatic pressures. On the other hand, Pugh's ratio is another pivotal parameter for determining whether the $CsSnCl_3$ perovskite material is ductile or brittle. The critical value considers as 1.75 [40], and if the value B/G exceeds the critical value, then the compound will be ductile, otherwise brittle [41]. From Tables 1, 2 we see that the perovskite compound of $CsSnCl_3$ has no brittle nature. The pressure, therefore, has enhanced the ductile behavior of $CsSnCl_3$.

Another important parameter in deciding the brittle and ductile condition of $CsSnCl_3$ is the Poisson's ratio ν, which has a critical value of 0.26, over which the material becomes ductile [41]. The computed value of ν of $CsSnCl_3$ at ambient conditions is 0.278 as listed in Table 1, which suggests the ductile nature of the $CsSnCl_3$. The pressure reduces the interatomic distance and increases the value of Poisson's ratio. As a consequence, the ductility of the perovskite compound $CsSnCl_3$ increases

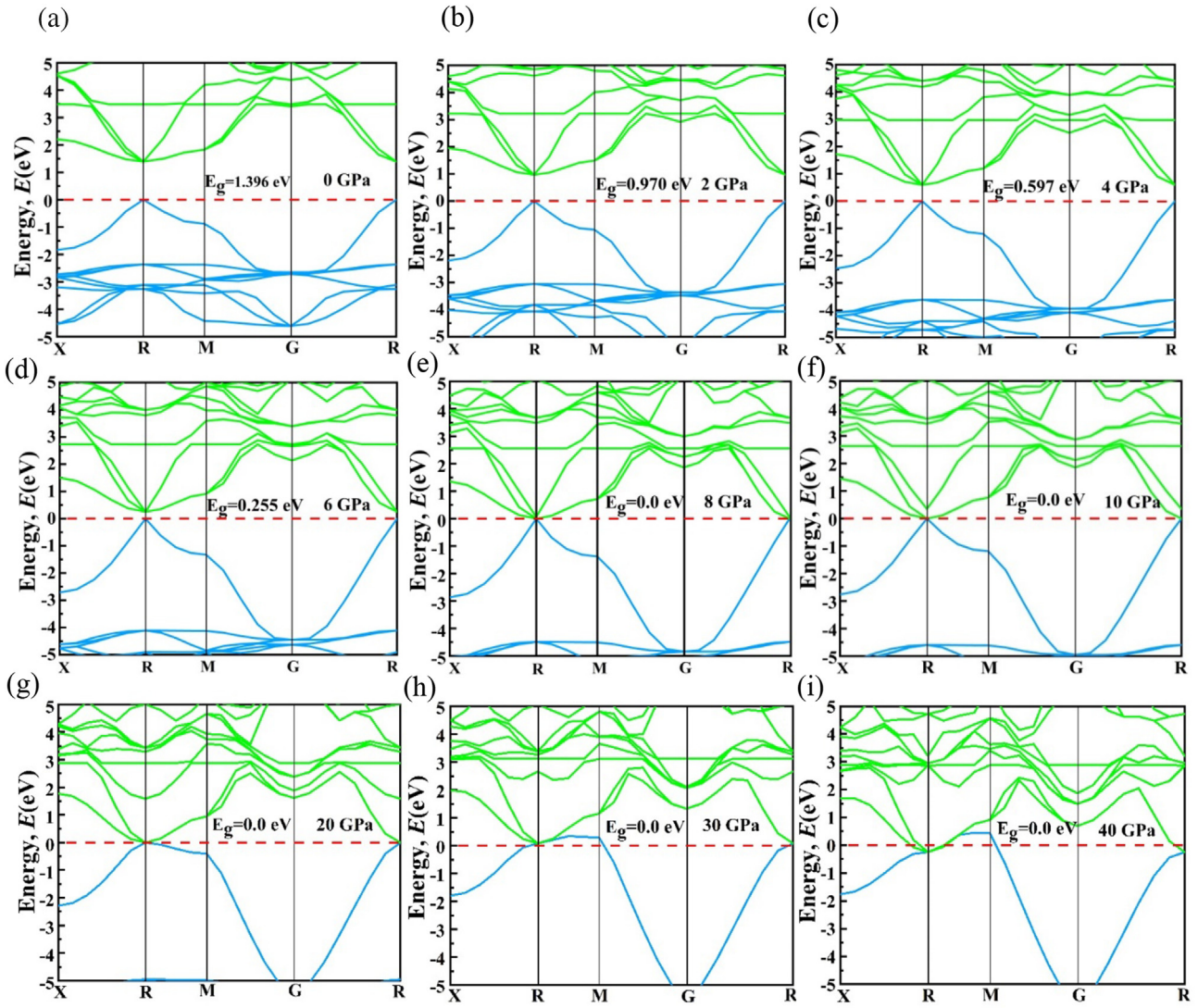

Figure 4. The computed band structure, by rPBE functional, of $CsSnCl_3$ under different pressures: (a) 0 GPa, (b) 2 GPa, (c) 4 GPa, (d) 6 GPa, (e) 8 GPa, (f) 10 GPa, (g) 20 GPa, (h) 30 GPa, and (i) 40. The dashed line at the zero-energy represents the Fermi level.

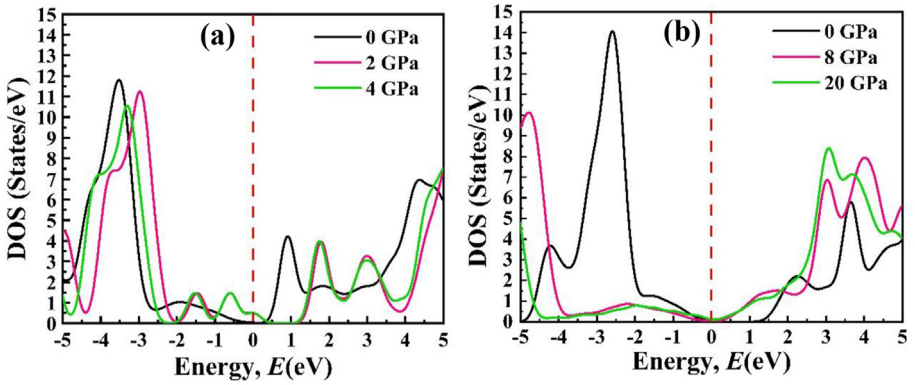

Figure 5. Calculated total electronic density of states of $CsSnCl_3$ under various pressures by using: (a) PBEsol and (b) rPBE) functionals. The dashed line at zero energy is the Fermi level.

with hydrostatic pressure. Generally, the mechanical hardness of a compound is directly related to Poisson's ratio [42], so it is expected that the hardness might also be increased with the pressure. The computed elastic constants and elastic moduli by using rPBE functional are listed in Table 2. The C_{11} and C_{44} strongly depend on the functional type, while C_{22} shows almost independent of functional. Interestingly, the compound is mechanically stable up to 40 GPa for rPBE functional, as the functional overestimates the experimental lattice parameters by 3.4 %.

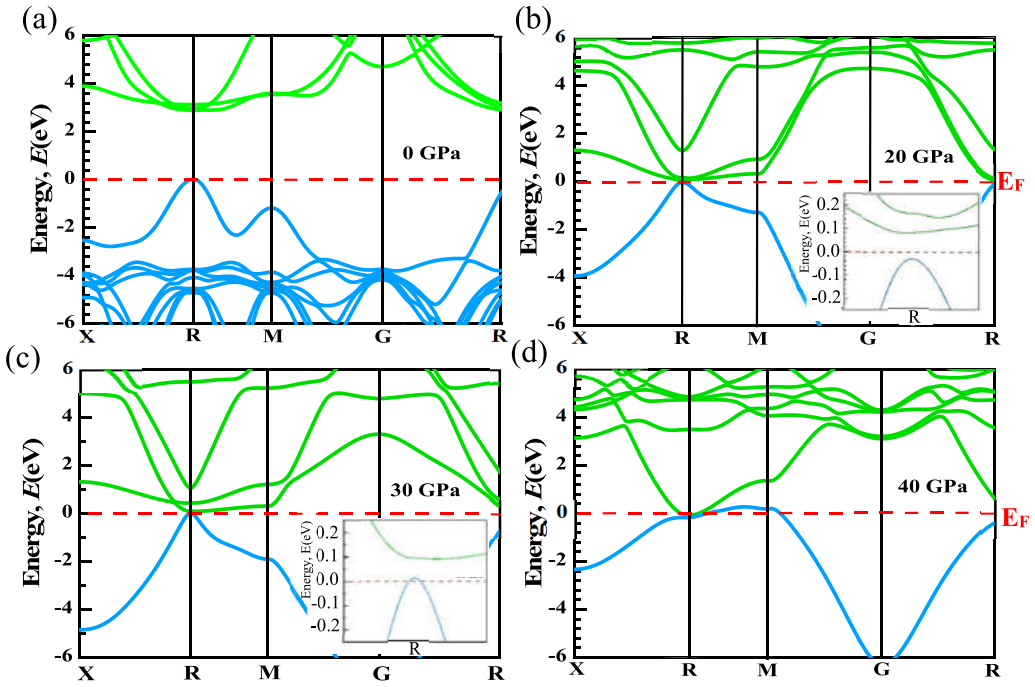

Figure 6. The computed band structure, by GW method, of $CsSnCl_3$ under pressure: (a) 0 GPa, (b) 20 GPa, (c) 30 GPa, and (d) 40 GPa. The dashed line at the zero-energy represents the Fermi level.

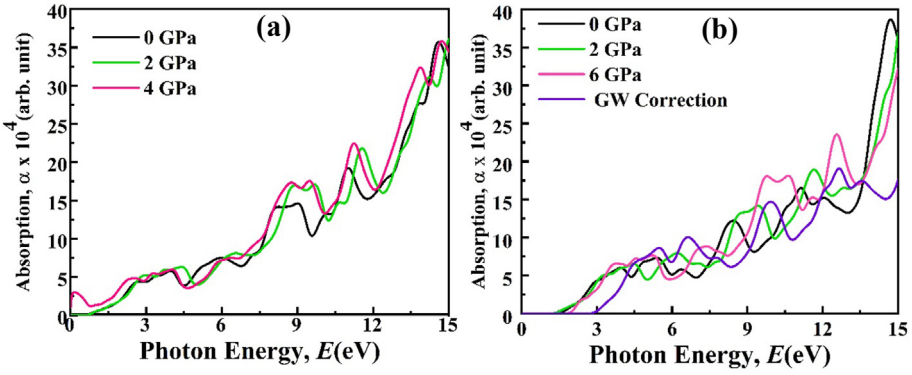

Figure 7. Calculated optical absorption of perovskite $CsSnCl_3$ as a (a) PBEsol and (b) rPBE functionals and with GW bandgap correction.

Table 1. Computed values of elastic constants C_{ij} (GPa), Cauchy pressure C_{12}–C_{44} (GPa), bulk modulus B (GPa), shear modulus G (GPa), and Poisson ration ν, of the cubic perovskite $CsSnCl_3$ under variant pressures by using PBEsol functional.

Pressure (GPa)	C_{11}	C_{12}	C_{44}	C_{12}–C_{44}	B (GPa)	G (GPa)	B/G	ν
0	58.98	9.18	5.59	3.59	25.78	13.31	1.94	0.28
2	77.94	12.31	5.40	6.91	34.19	16.37	2.09	0.29
4	95.65	15.61	5.16	10.45	42.29	19.10	2.21	0.30
6	112.71	19.15	4.88	14.27	50.34	21.64	2.33	0.31
8	128.34	22.58	4.58	18.00	57.83	23.9	2.42	0.32
10	143.58	26.03	4.24	21.79	65.21	26.05	2.50	0.32
20	213.83	44.96	2.38	42.58	101.25	35.20	2.88	0.34
30	275.41	63.99	0.19	63.8	134.46	42.40	3.17	0.36
40	334.83	86.69	-2.2	88.9	169.40	48.30	3.51	0.37

4. Conclusions

In summary, we have studied the structural, electronic, absorption coefficient, and mechanical properties of cubic $CsSnCl_3$ compound at different pressures by using the first-principles method based on the density functional theory (DFT). We used PBEsol, rPBE functionals, and the accurate GW method and found that the PBEsol gives the lattice parameters close to the experimental value compared to that of rPBE

Table 2. Calculated values of C_{ij} (GPa), Cauchy pressure C_{12}–C_{44} (GPa), bulk modulus B (GPa), shear modulus G (GPa), and Poisson ration ν of cubic $CsSnCl_3$ perovskite under variant pressures by using rPBE functional.

Pressure (GPa)	C_{11}	C_{12}	C_{44}	C_{12}–C_{44}	B (GPa)	G (GPa)	B/G	ν
0	39.47	9.04	6.51	2.53	19.19	10.00	1.92	0.278
2	58.15	12.48	6.58	5.90	27.70	13.08	2.12	0.296
4	74.15	15.57	6.53	9.04	35.10	15.63	2.25	0.306
6	90.37	18.77	6.42	12.35	42.64	18.17	2.35	0.313
8	105.95	21.75	6.25	15.50	49.82	20.59	2.42	0.318
10	121.68	24.84	6.05	18.79	57.12	23.00	2.48	0.322
20	188.98	41.14	4.68	36.46	90.42	32.38	2.79	0.340
30	250.21	58.71	2.93	55.78	122.54	40.06	3.06	0.352
40	306.15	76.64	0.88	75.76	153.14	46.43	3.30	0.362

functional. However, the underestimation of the bandgap is more severe in the case of PBEsol functional than rPBE. The GW method gives the most accurate bandgap of 2.91 eV at ambient conditions, which is in excellent agreement with the experimentally measured bandgap of 2.9 eV. Our calculations reveal that the predictions of semiconducting to metallic transitions strongly depend on the exchange-correlation term used in the calculations and the GW method can predict the most accurate among these approaches. However, the absorption coefficient of $CsSnCl_3$ improves slightly by applying pressure.

Declarations

Author contribution statement

Md.Majibul Haque Babu, Tusar Saha: Conceived and designed the experiments; Performed the experiments; Analyzed and interpreted the data; Wrote the paper.

Jiban Podder, Protima Roy, Abdul Barik: Analyzed and interpreted the data.

Enamul Haque: Performed the experiments; Analyzed and interpreted the data; Wrote the paper.

Funding statement

This research did not receive any specific grant from funding agencies in the public, commercial, or not-for-profit sectors.

Data availability statement

Data will be made available on request.

Declaration of interests statement

The authors declare no conflict of interest.

Additional information

No additional information is available for this paper.

References

[1] L. Huang, W.R.L. Lambrecht, Electronic band structure trends of perovskite halides: beyond Pb and Sn to Ge and Si, Phys. Rev. B 93 (2016) 195211.
[2] A. Koliogiorgos, C.S. Garoufalis, I. Galanakis, S. Baskoutas, Electronic and optical properties of ultrasmall ABX_3 (A= Cs, CH_3NH_3/B= Ge, Pb, Sn, Ca, Sr/X= Cl, Br, I) perovskite quantum dots, ACS Omega 3 (2018) 18917–18924.
[3] R. Ben Sadok, N. Plugaru, A. Birsan, V. Kuncser, D. Hammoutène, Effect of chemical nature of atoms on the electronic, dielectric, and dynamical properties of ABX_3 halide perovskite, Int. J. Quant. Chem. 120 (2020), e26172.
[4] B.-B. Deng, C.-C. Xu, T.-T. Cheng, Y.-T. Yang, Y.-T. Hu, P. Wang, W.-H. He, M.-J. Yang, W.-Q. Liao, Homochiral nickel nitrite ABX_3 (X= NO_2^-) perovskite ferroelectrics, J. Am. Chem. Soc. 142 (2020) 6946–6950.
[5] S. Körbel, M.A.L. Marques, S. Botti, Stability and electronic properties of new inorganic perovskites from high-throughput ab initio calculations, J. Mater. Chem. C. 4 (2016) 3157–3167.
[6] Q. Sun, W.-J. Yin, Thermodynamic stability trend of cubic perovskites, J. Am. Chem. Soc. 139 (2017) 14905–14908.
[7] M. Anaya, G. Lozano, M.E. Calvo, H. M'iguez, ABX_3 perovskites for tandem solar cells, Joule 1 (2017) 769–793.
[8] W.-J. Yin, T. Shi, Y. Yan, Unique properties of halide perovskites as possible origins of the superior solar cell performance, Adv. Mater. 26 (2014) 4653–4658.
[9] L.N. Quan, B.P. Rand, R.H. Friend, S.G. Mhaisalkar, T.-W. Lee, E.H. Sargent, Perovskites for next-generation optical sources, Chem. Rev. 119 (2019) 7444–7477.
[10] Y.-Q. Zhao, Q.-R. Ma, B. Liu, Z.-L. Yu, M.-Q. Cai, Pressure-induced strong ferroelectric polarization in tetra-phase perovskite $CsPbBr_3$, Phys. Chem. Chem. Phys. 20 (2018) 14718–14724.
[11] T. Ou, J. Yan, C. Xiao, W. Shen, C. Liu, X. Liu, Y. Han, Y. Ma, C. Gao, Visible light response, electrical transport, and amorphization in compressed organolead iodine perovskites, Nanoscale 8 (2016) 11426–11431.
[12] G. Liu, L. Kong, P. Guo, C.C. Stoumpos, Q. Hu, Z. Liu, Z. Cai, D.J. Gosztola, H. Mao, M.G. Kanatzidis, others, Two regimes of bandgap red shift and partial ambient retention in pressure-treated two-dimensional perovskites, ACS Energy Lett. 2 (2017) 2518–2524.
[13] D.Z. Metin, N. Gaston, Internal and external pressure in cubic perovskites: electronic structure effects and systematic accuracy from first principles, Electron. Struct. 1 (2019) 35001.
[14] W.-J. Yin, J.-H. Yang, J. Kang, Y. Yan, S.-H. Wei, Halide perovskite materials for solar cells: a theoretical review, J. Mater. Chem. A. 3 (2015) 8926–8942.
[15] Y. Jiao, S. Yi, H. Wang, B. Li, W. Hao, L. Pan, Y. Shi, X. Li, P. Liu, H. Zhang, others, Strain Engineering of metal halide perovskites on coupling anisotropic behaviors, Adv. Funct. Mater. 31 (2021) 2006243.
[16] Q. Ou, X. Bao, Y. Zhang, H. Shao, G. Xing, X. Li, L. Shao, Q. Bao, Band structure engineering in metal halide perovskite nanostructures for optoelectronic applications, Nano Mater. Sci. 1 (2019) 268–287.
[17] U. Schwarz, F. Wagner, K. Syassen, H. Hillebrecht, Effect of pressure on the optical-absorption edges of $CsGeBr_3$ and $CsGeCl_3$, Phys. Rev. B 53 (1996) 12545.
[18] D.-K. Seo, N. Gupta, M.-H. Whangbo, H. Hillebrecht, G. Thiele, Pressure-induced changes in the structure and band gap of $CsGeX_3$ (X= Cl, Br) studied by electronic band structure calculations, Inorg. Chem. 37 (1998) 407–410.
[19] J. Islam, A.K.M.A. Hossain, Semiconducting to metallic transition with outstanding optoelectronic properties of $CsSnCl_3$ perovskite under pressure, Sci. Rep. 10 (2020) 1–11.
[20] Y. Ying, X. Luo, H. Huang, Pressure-induced topological nontrivial phase and tunable optical properties in all-inorganic halide perovskites, J. Phys. Chem. C 122 (2018) 17718–17725.
[21] M.D. Segall, P.J.D. Lindan, M.J. Probert, C.J. Pickard, P.J. Hasnip, S.J. Clark, M.C. Payne, First-principles simulation: ideas, illustrations and the CASTEP code, J. Phys. Condens. Matter. 14 (2002) 2717–2744.
[22] K. Refson, CASTEP user guide, CCLRC Rutherford Applet. Lab, 2004.
[23] D. Vanderbilt, Soft self-consistent pseudopotentials in a generalized eigenvalue formalism, Phys. Rev. B 41 (1990) 7892.
[24] T.H. Fischer, J. Almlof, General methods for geometry and wave function optimization, J. Phys. Chem. 96 (1992) 9768–9774.
[25] H.J. Monkhorst, J.D. Pack, Special points for Brillouin-zone integrations, Phys. Rev. B 13 (1976) 5188.
[26] F.D. Murnaghan, Finite deformations of an elastic solid, Am. J. Math. 59 (1937) 235–260.
[27] P. Giannozzi, S. Baroni, N. Bonini, M. Calandra, R. Car, C. Cavazzoni, D. Ceresoli, G.L. Chiarotti, M. Cococcioni, I. Dabo, others, QUANTUM ESPRESSO: a modular and open-source software project for quantum simulations of materials, J. Phys. Condens. Matter. 21 (2009) 395502.
[28] M.J. Van Setten, M. Giantomassi, E. Bousquet, M.J. Verstraete, D.R. Hamann, X. Gonze, G.-M. Rignanese, The PseudoDojo: training and grading a 85 element optimized norm-conserving pseudopotential table, Comput. Phys. Commun. 226 (2018) 39–54.
[29] D.R. Hamann, Optimized norm-conserving Vanderbilt pseudopotentials, Phys. Rev. B 88 (2013) 85117.
[30] J. Deslippe, G. Samsonidze, D.A. Strubbe, M. Jain, M.L. Cohen, S.G. Louie, BerkeleyGW, a massively parallel computer package for the calculation of the

quasiparticle and optical properties of materials and nanostructures, Comput. Phys. Commun. 183 (2012) 1269–1289.
[31] J. Barrett, S.R.A. Bird, J.D. Donaldson, J. Silver, The Mössbauer effect in tin (II) compounds. Part XI. The spectra of cubic trihalogenostannates (II), J. Chem. Soc. A Inorganic Phys. Theor. (1971) 3105–3108.
[32] A.S. Voloshinovskii, S. V Myagkota, N.S. Pidzyrailo, M. V Tokarivskii, Luminescence and structural transformations of $CsSnCl_3$ crystals, J. Appl. Spectrosc. 60 (1994) 226–228.
[33] L. Peedikakkandy, P. Bhargava, Composition dependent optical, structural and photoluminescence characteristics of cesium tin halide perovskites, RSC Adv. 6 (2016) 19857–19860.
[34] L. Huang, W.R.L. Lambrecht, Electronic band structure, phonons, and exciton binding energies of halide perovskites $CsSnCl_3$, $CsSnBr_3$, and $CsSnI_3$, Phys. Rev. B 88 (2013) 165203.
[35] W. Shockley, H.J. Queisser, Detailed balance limit of efficiency of p-n junction solar cells, J. Appl. Phys. 32 (1961) 510–519.
[36] J. Wang, Y. Zhou, Dependence of elastic stiffness on electronic band structure of nanolaminate M_2A1C (M=Ti,V,Nb, and Cr) ceramics, Phys. Rev. B 69 (2004) 1–9.
[37] F. Mouhat, F.-X. Coudert, Necessary and sufficient elastic stability conditions in various crystal systems, Phys. Rev. B 90 (2014) 224104.
[38] N. Korozlu, K. Colakoglu, E. Deligoz, Y.O. Ciftci, The structural, electronic and optical properties of $Cd_xZn_{1-x}Se$ ternary alloys, Opt. Commun. 284 (2011) 1863–1867.
[39] A. Reuss, Calculation of the flow limits of mixed crystals on the basis of the plasticity of monocrystals, Z. Angew. Math. Mech. 9 (1929) 49–58.
[40] R. Hill, The elastic behaviour of a crystalline aggregate, Proc. Phys. Soc. Sect. A. 65 (1952) 349–354.
[41] S.F. Pugh, XCII. Relations between the elastic moduli and the plastic properties of polycrystalline pure metals, London, Edinburgh, Dublin Philos. Mag. J. Sci. 45 (1954) 823–843.
[42] R. Hill, The elastic behaviour of a crystalline aggregate, Proc. Phys. Soc. Sect. A. 65 (1952) 349.